Uncertainty quantification and global sensitivity analysis of piezoelectric energy harvesting using macro fiber composites

Rabie Aloui, Walid Larbi, Mnaouar Chouchane

Uncertainty quantification and global sensitivity analysis of piezoelectric energy harvesting using macro fiber composites

Rabie Aloui[1,2], **Walid Larbi**[2] **and Mnaouar Chouchane**[1]

[1] Université de Monastir, École Nationale d'Ingénieurs de Monastir, Laboratoire de Génie Mécanique, LA-MA-05, Monastir, Tunisia
[2] Structural Mechanics and Coupled Systems Laboratory (LMSSC), Conservatoire National des Arts et Métiers (CNAM), Paris, France

E-mail: rabie.aloui@enim.rnu.com, walid.larbi@cnam.fr and mnaouar.chouchane@enim.rnu.tn

Abstract

Piezoelectric macro fiber composites (MFCs) are widely used for energy harvesting due to their flexibility and high electromechanical conversion efficiency. In previous research studies, numerical and analytical models have been developed for MFC-harvesters using homogenized electromechanical properties. In this paper, an analytical electroelastic coupled model, based on the mixing rules, is used to predict the output responses of an MFC-harvester coupled in 33-mode of the PZT fibers. The predicted responses exhibit variation because of the uncertainty of the parameters used in the proposed model. The research reported in this paper aims to estimate the effect of the uncertainty in the physical properties of both piezoelectric fibers and epoxy matrix on the model responses and to identify the parameters which cause large output variability. The uncertainties of the parameters are defined as the variability bounds based on the tolerances reported by the manufacturers. Global sensitivity analysis (GSA) is an appropriate method to study the effect of the uncertainty of parameters on the electromechanical response of the harvester. Two GSA are applied in this paper: *(i)* the Morris method based on the elementary effects measures and *(ii)* the variance method which consists in computing the Sobol' indices, whose goal is to identify systems parameters which have significant impact on the voltage and the power outputs of a bimorph MFC-harvester. This study leads to a qualitative comparison between the two methods which are strategically different. Both methods indicate that the elastic modulus and the density of the piezoelectric fibers, the length and the thickness of the representative volume element of the MFC-patch are the most influential parameters that affect the output voltage. It has also been shown that the order of importance of the parameters can change from the short-circuit to the open-circuit condition. Furthermore, Monte Carlo simulations are used to propagate the uncertainties of the parameters in order to determine the envelope of the variability of the responses. This study reveals the importance of considering model parameter uncertainties in the development of robust prediction tools for piezoelectric energy harvesting devices.

Keywords: Global sensitivity analysis, Stochastic prediction, Piezoelectric energy harvesting, Macro fiber composites

1. Introduction

Smart materials such as piezoelectric, magnetostrictive and shape memory alloys have recently found an increasing interest in several engineering applications including shape control, energy harvesting, vibration control and structural health monitoring [1, 2]. In particular, piezoelectric materials are widely applied in engineering applications due to their beneficial features, especially for vibration attenuation [3–5] and vibration energy harvesting [6]. Piezoceramics, commonly used piezoelectric materials, are brittle and susceptible to fracture during handling and bonding procedures. Moreover, these materials cause often a high structural stiffness, which is not desirable for large strain applications or when the material in a patch form is bonded to curved surfaces. Consequently, researchers developed composite materials based on piezoelectric materials to reduce these limitations.

Macro fiber composites using piezoceramic fibers, developed by NASA Langley Research Center [7–9], have been used for many sensing and actuation applications because of their beneficial flexibility features and integration easiness compared to the monolithic piezoceramic patches. An MFC-patch consists of monolithic piezoceramic fibers embedded in a polymer matrix covered by inter-digitated electrodes on the top and bottom surfaces of the composite patch [10]. Many research studies on analytical and numerical modeling of MFCs have focused on homogenization and characterization of the mechanical and electrical properties [9, 11–13]. The modeling of the MFC-patches is more delicate than that of monolithic piezoelectric patches because of the non-uniform and piece-wise defined electric field when the piezoelectric 33-mode is used. Erturk *et al* [14] investigated piezoelectric energy harvesting capabilities using MFC patches for morphing of aircraft wings subjected to air flow excitation. A subsequent experimental study confirmed the results obtained from the analytical modeling. Song *et al* [15, 16] presented a parametric analytical study of an MFC-harvester subjected to harmonic base excitation. This research was performed to gain insight into methods to maximize the electrical generated power and current by varying the physical parameters of the harvester. Both 31- and 33-coupling modes of the MFC patches are considered and harvester responses are determined for different levels of base acceleration. The results obtained in this study show that the d33-type produced a slightly higher power. However, the d31-type generated higher maximum current. This means that the d31-type may be a better choice than the d33-type MFC for energy storage applications. Bilgen *et al* [17] proposed a linear distributed parameter electromechanical model to predict the actuated structural response of clamped-free MFC unimorph beams. The model is applied to determine the response of the MFC harvester for various substrate materials and substrate thicknesses. The authors confirmed experimentally their theoretical findings. Shahab *et al* [18] investigated the electroelastic coupling of a bimorph MFC-harvester which employs interdigitated electrodes and the 33-mode coupling. The developed distributed-parameter model using equivalent electromechanical properties obtained from the rules of mixture, is applied for different elastodynamic scenarios of piezoelectric power generation and dynamic actuation. A good concordance agreement is reported compared to experimental electrical and mechanical responses.

Sensitivity analysis has long been considered an effective method for better study of mechatronic systems. This method of analysis is applied to determine the sensitivity of the model responses to uncertainties of the input parameters. The classical approach of sensitivity analysis, known as the local approach, considers the impact of small perturbations of the inputs around nominal values on the model output [19–24]. For instance, Aloui *et al* [25] investigated the first order sensitivity analysis of complex frequency response functions of piezoelectric energy harvesters based on the finite difference approach to evaluate the electromechanical outputs to small variations of the load resistance. In contrast to local sensitivity analysis, the global sensitivity analysis overcomes the limitations of the first local sensitivity by considering the whole range of variation of the inputs [26]. Ruiz *et al* [27] analyzed the global sensitivity of the voltage frequency response function of several configurations of piezoelectric energy harvesters. The approach applied in this research is based on the variance decomposition which yields Sobol indices to assess the robustness of the stochastic prediction. Aloui *et al* [28] applied the Elementary Effects method (EEs) as a particular implementation of the global sensitivity method to identify the impact of substrate and piezoelectric material properties on the voltage frequency response function of a typical bimorph piezoelectric energy harvester with fixed geometry. Kucherenko *et al* [29] presented a novel approach of the derivative-based global sensitivity measures. The proposed method is then compared to the Morris and Sobol' indices to reveal a close link between the proposed method and Sobol' sensitivity approach.

The electromechanical modeling of MFC material is widely investigated in several published researches; however, few studies focused on the sensitivity analysis as a technique for the input/output characterization of the MFC-system. In this paper, we propose an in-depth characterization of an MFC-harvester using the 33-mode of electromechanical coupling, which is recently introduced for energy harvesting applications, based on the global sensitivity analysis of the output responses to its physical properties. Furthermore, uncertainty analysis is applied to validate the computational results obtained using the sensitivity analysis. Monte Carlo simulation method is thus applied to calculate the propagation of uncertainties of parameters to the output voltage of the harvester in both short- and open-circuit conditions.

This research paper is organized into six sections. Following this introduction, an analytical modeling of a vibration energy harvester using piezoceramic MFC patches is introduced in section 2 to derive the complex frequency response functions. A brief review on two global sensitivity analysis methods are presented in section 3, which are: *(i)* the Elementary Effects method (EEs) [30] and *(ii)* the variance-based sensitivity analysis used to determine the Sobol' indices [31]. These two methods are given in terms of the model output responses. Section 4 presents the principles of stochastic

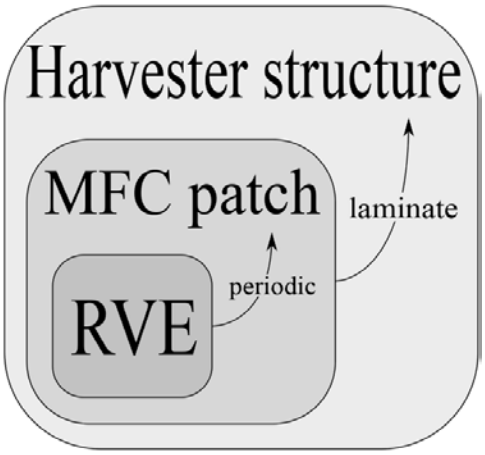

Figure 1. A schematic of the modeling strategy from representative volume element (RVE) of an MFC-patch to the MFC-harvester laminated beam.

prediction and the propagation of the uncertainty on the input parameters to the model outputs. A numerical example is presented in section 5 providing a comparison between the two GSA methods. The uncertainty quantification is applied in this section for robustness stochastic prediction analysis. These two sensitivity analysis approaches are applied on a bimorph MFC-harvester considered as a case study in this paper. The paper is concluded in section 6.

2. Analytical modeling of a piezoceramic MFC-harvester

The electromechanical modeling of a piezoelectric energy harvester is based on the distributed parameter model introduced by Erturk and Inman [32, 33]. The model is developed for both unimorph and bimorph cantilever beams with a monolithic piezoceramic layers subjected to base excitation. The modeling strategy starts from a representative volume element (RVE) to build the periodical structure of the MFC-patch in both transverse and longitudinal directions as illustrated in figure 1, then the patch model is incorporated into the laminated MFC-harvester.

The modeling of the coupled distributed parameter problem of the MFC-harvester is based on the following assumptions:

- The model is based on Euler-Bernoulli beam theory; i.e. shear deformations and rotary inertia effects are neglected. Note that the thickness and the width of the structure are small compared to its length, which justifies the use of the beam theory.
- The deformation of the substrate and piezoceramic patches are assumed to be linear elastic following Hooke's law.
- The interdigitated electrodes of the patches are assumed to have negligible mass and stiffness contribution to the harvester. Hence, the harvester is assumed to be uniform in the length direction.

The MFC-patch is composed of uni-axially aligned piezoelectric fibers embedded into a polymer matrix. The fibers have rectangular cross-sections as shown in figure 2. Furthermore, the MFC patch includes interdigitated electrodes for adaptation to the electric field along the length of the fibers and to provide a supporting structure for the harvester.

2.1. Electromechanical modeling of the MFC-patch

The MFC-patch is assumed to be a symmetric laminate composed of a PZT-epoxy composite layer covered by two interdigitated electrodes layers on the top and the bottom surfaces of the composite layer. The PZT fibers are traditionally oriented parallel to the x-direction while the electrodes are aligned in the transverse direction (the y-direction). The MFC-patch is a periodical structure of a representative volume element in both x- and y-directions as shown in figure 2. The patch is composed of $(N \times M)$ RVEs respectively in the length and width directions; i.e. N and M are respectively the number of electrode pairs and the number of PZT fibers.

The piezoceramic fibers of the MFC-patch obey the following linear constitutive equations based on the Euler-Bernoulli beam assumptions and the 33-mode of electromechanical coupling [18]:

$$\sigma_3 = \bar{c}^E_{33,e}\varepsilon_3 - \bar{e}_{33,e}E_3 \tag{1a}$$

$$D_3 = \bar{e}_{33,e}\varepsilon_3 + \bar{\epsilon}^S_{33,e}E_3 \tag{1b}$$

where σ_3 is the stress, ε_3 is the strain, E_3 is the electric field, D_3 is the electric displacement, $\bar{c}^E_{33,e}$ is the elastic modulus at constant electric field, $\bar{e}_{33,e}$ is the effective piezoelectric stress constant, $\bar{\epsilon}^S_{33,e}$ is the permittivity component at constant strain. The subscript e stands for the equivalent properties which are defined based on mixing rules formulation for an RVE as follows:

$$\bar{c}^E_{33,e} = \nu\bar{c}^E_{33,p} + (1-\nu)\bar{c}^E_{33,m} \tag{2}$$

$$\bar{d}_{33,e} = \left(\frac{1}{\bar{c}^E_{33,e}}\right)\nu\bar{d}_{33,p}\bar{c}^E_{33,p} \tag{3}$$

$$\bar{\epsilon}^S_{33,e} = \left[\nu\bar{\epsilon}^\sigma_{33,p} + (1-\nu)\bar{\epsilon}^\sigma_{33,m}\right] - \left(\bar{d}_{33,e}\right)^2\bar{c}^E_{33,e} \tag{4}$$

where the subscripts p and m refer respectively to the piezoelectric fibers and the polymer matrix, ν is the fiber to matrix volume ratio and $\bar{\epsilon}^\sigma_{33}$ is the permittivity component at constant stress. Furthermore, the piezoelectric strain coefficient $\bar{d}_{33,e}$ can be expressed in terms of the more common piezoelectric stress constant as follows:

$$\bar{d}_{33,e} = \frac{\bar{e}_{33,e}}{\bar{c}^E_{33,e}} \tag{5}$$

Although the electric field is non-uniform within the piezoceramic fibers as shown in figure 2(b), the electric field in the 33-mode of electromechanical coupling can be approximated by:

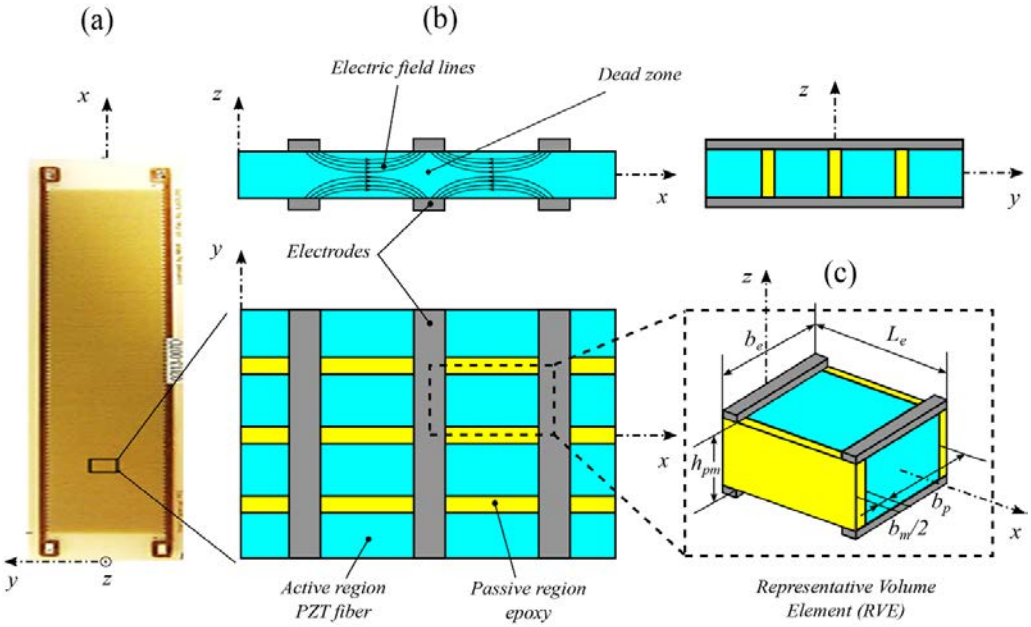

Figure 2. (a) An MFC-patch, (b) a representative part of the MFC-patch showing the PZT fibers with the electric field lines separated by the polymer matrix and the interdigitated electrodes in the 33-mode of electromechanical coupling of piezoelectricity and (c) an RVE of symmetric shape.

$$E_3 \approx \frac{\pm v(t)}{L_e} \tag{6}$$

where $v(t)$ is the voltage across the interdigitated electrodes and L_e is the distance between two subsequent electrodes (i.e. the length of the RVE) as shown in figure 2.

2.2. Electromechanical coupling under base excitation

The transverse displacement of the beam can be expressed as:

$$w(x,t) = w_b(t) + w_{rel}(x,t) \tag{7}$$

where $w_{rel}(x,t)$ is the transverse displacement relative to base motion $w_b(t)$. Expressing the strain component in terms of the curvature and the electric field in terms of the voltage and substituting equation (7) into the governing partial differential equation of free vibration of the cantilevered harvester gives the following forced partial differential equation for the relative response $w_{rel}(x,t)$ [33, 34]:

$$\begin{aligned} &YI\frac{\partial^4 w_{rel}(x,t)}{\partial x^4} + c_s I\frac{\partial^5 w_{rel}(x,t)}{\partial x^4 \partial t} \\ &+ c_a\frac{\partial w_{rel}(x,t)}{\partial t} + m\frac{\partial^2 w_{rel}(x,t)}{\partial t^2} + v(t)\frac{d^2\Gamma(x)}{dx^2} = \\ &- m\frac{\partial^2 w_b(t)}{\partial t^2} - c_a\frac{\partial w_b(x,t)}{\partial t} \end{aligned} \tag{8}$$

where c_s and c_a are respectively the strain rate damping coefficient and the viscous air damping coefficient, YI is the bending stiffness which is obtained from the equivalent properties of the laminates, given by the mixing rules, and the parallel axis theorem, m is the mass per unit length of the beam which must account for all the material density entities in a transverse section and $\Gamma(x)$ accounts for the spatial distribution of the electric potential:

$$\Gamma(x) = \vartheta\sum_{n=1}^{N}[H(x-(n-1)L_e) - H(x-nL_e)] \tag{9}$$

where $H(x)$ is the Heaviside function, and nth is the index of the RVE located at a distance x from the fixed end of the bimorph, N is the number of RVEs in the x-direction (number of pairs of electrodes) in the active length $L = N \times L_e$ of the MFC-patch and ϑ is the backward coupling coefficient which can be expressed as follows:

$$\vartheta = M\bar{d}_{33,e}\bar{c}^E_{33,e}\frac{A_e}{L_e}h_{pc} = M\bar{e}_{33,e}\frac{A_e}{L_e}h_{pc} \tag{10}$$

where h_{pc} is the distance from the neutral axis to the center of the piezoceramic, and A_e is the effective surface area which is introduced to account for the approximation of the electric field [35]. Furthermore, the effective area corresponds to the contact area between the electrodes and the piezoceramic fiber (i.e. the effective electrode area).

The equation for the electrical output voltage is obtained by using the integral form of Gauss's law and the constitutive equation (1b), as follows:

$$C\frac{dv(t)}{dt} - \frac{v(t)}{R} + \vartheta\int_0^L \frac{\partial^3 w_{rel}(x,t)}{\partial x^2 \partial t}dx = 0 \tag{11}$$

where C is the capacitance of the MFC-patch; assuming that the capacitance of the interdigitated electrodes is negligible [36]. This capacitance is expressed as follows [37]:

$$C = \sum_{m=1}^{M}\sum_{n=1}^{N} \overline{\epsilon}^{S}_{33,e}\frac{A_e}{L_e} = MN\overline{\epsilon}^{S}_{33,e}\frac{A_e}{L_e} \tag{12}$$

2.3. Modal analysis of the harvester

The vibration response of an MFC-harvester relative to its base can be expressed in terms of the eigenfunctions as follows:

$$w_{rel}(x,t) = \sum_{r=1}^{\infty} \phi_r(x) q_r(t) \tag{13}$$

where $\phi_r(x)$ and $q_r(t)$ are respectively the mass normalized eigenfunction and the modal mechanical coordinate of the clamped-free beam for the r^{th} mode. The eigenfunction of the undamped system is:

$$\phi_r(x) = \sqrt{\frac{1}{mL}}\left[\cosh\frac{\lambda_r}{L}x - \cos\frac{\lambda_r}{L}x - \varrho_r\left(\sinh\frac{\lambda_r}{L}x - \sin\frac{\lambda_r}{L}x\right)\right] \tag{14}$$

where the dimensionless eigenvalues λ_r are obtained from the following characteristic equation:

$$1 + \cos\lambda\cosh\lambda = 0 \tag{15}$$

and ϱ_r is expressed as:

$$\varrho_r = \frac{\sinh\lambda_r - \sin\lambda_r}{\cosh\lambda_r + \cos\lambda_r} \tag{16}$$

The natural frequency for the r^{th} mode ω_r is related to the λ_r as follows:

$$\omega_r = \lambda_r^2\sqrt{\frac{YI}{mL^4}} \tag{17}$$

which corresponds approximately to the r^{th} resonance frequency of the structure when the MFC-harvester is in short circuit condition. The mass-normalized eigenfunctions satisfy the following orthogonality conditions [38]:

$$\int_{x=0}^{L} m\phi_s(x)\phi_r(x)dx = \delta_{rs} \quad \text{and} \quad \int_{x=0}^{L} YI\phi_s(x)\frac{d^4\phi_r(x)}{dx^4}dx = \omega_r^2\delta_{rs} \tag{18}$$

where δ_{rs} is the Kronecker delta function which is equal to 1 if $r = s$, and 0 otherwise.

2.4. Steady state frequency responses functions of the MFC-harvester

Considering a harmonic steady-state modal mechanical response $q_r(t) = q_r e^{j\omega t}$ and voltage response $v(t) = ve^{j\omega t}$ for an excitation due to a harmonic base excitation $w_b(t) = w_b e^{j\omega t}$ and transforming Equations (8) and (11) to the frequency domain using the modal expansion in equation (13) yields:

$$(\omega_r^2 - \omega^2 + j2\zeta_r\omega_r\omega)q_r - \theta_r v = f_r(t) \tag{19a}$$

$$\left(\frac{1}{R} + j\omega C\right)v + j\omega\sum_{r=1}^{\infty}\theta_r q_r = 0 \tag{19b}$$

where ζ_r is the modal mechanical damping ratio which is defined as follows:

$$\zeta_r = \frac{c_s I\omega_r}{2YI} + \frac{c_a}{2\,m\omega_r} \tag{20}$$

The modal electromechanical coupling term of the MFC-patch is defined as follows:

$$\theta_r = M\overline{e}_{33,e}\frac{A_e}{L_e}h_{pc}\frac{d\phi_r(x)}{dx}|_{x=L} = \vartheta\frac{d\phi_r(x)}{dx}|_{x=L} \tag{21}$$

and the modal force is expressed as $f_r(t)$ which is defined as follows:

$$f_r(t) = \left(-m\int_0^L \phi_r(x)dx\right)\ddot{w}_b(t) = -\sigma_r\ddot{w}_b(t) \tag{22}$$

where σ_r is the modal effective mass of the harvester.

The association of two identical MFC-patches, either in series or in parallel connection with the electrical circuit makes it possible to write an equivalent problem with equivalent terms. Table 1 presents the equivalent modal electromechanical coupling and the equivalent capacitance for the series and parallel connections.

Thus, the FRFs for the voltage output-to-base acceleration of the bimorph MFC-harvester can be expressed as [32, 37]:

$$\frac{v(t)}{-\omega^2 w_b e^{j\omega t}} = \frac{\sum_{r=1}^{\infty}\frac{-j\omega\theta_r^{eq}\sigma_r}{\omega_r^2-\omega^2+j2\zeta_r\omega_r\omega}}{\frac{1}{R} + j\omega C^{eq} + \sum_{r=1}^{\infty}\frac{j\omega\theta_r^{eq\,2}}{\omega_r^2-\omega^2+j2\zeta_r\omega_r\omega}} \tag{23}$$

The relative tip displacement-to-base acceleration FRF, as a function of the voltage FRF, is:

$$\frac{w_{rel}(L,t)}{-\omega^2 w_b e^{j\omega t}} = \sum_{r=1}^{\infty}\left[\left(\sigma_r - \theta_r^{eq}\frac{\sum_{r=1}^{\infty}\frac{-j\omega\theta_r^{eq}\sigma_r}{\omega_r^2-\omega^2+j2\zeta_r\omega_r\omega}}{\frac{1}{R} + j\omega C^{eq} + \sum_{r=1}^{\infty}\frac{j\omega\theta_r^{eq\,2}}{\omega_r^2-\omega^2+j2\zeta_r\omega_r\omega}}\right)\frac{\phi_r(L)}{\omega_r^2 - \omega^2 + j2\zeta_r\omega_r\omega}\right] \tag{24}$$

Table 1. The equivalent modal electromechanical coupling and capacitance of a bimorph MFC-harvester for the series and parallel connections of the MFC-patchs.

	Series connection	Parallel connection
θ_r^{eq}	θ_r	$2\theta_r$
C^{eq}	$\frac{C}{2}$	$2\,C$

The electrical power FRF can be derived from the voltage FRF for a given external load resistance as follows:

$$\frac{P(t)}{\left(-\omega^2 w_b e^{j\omega t}\right)^2} = \frac{1}{R}\left(\frac{\sum_{r=1}^{\infty}\frac{-j\omega\theta_r^{eq}\sigma_r}{\omega_r^2-\omega^2+j2\zeta_r\omega_r\omega}}{\frac{1}{R}+j\omega C^{eq}+\sum_{r=1}^{\infty}\frac{j\omega\theta_r^{eq2}}{\omega_r^2-\omega^2+j2\zeta_r\omega_r\omega}}\right)^2 \tag{25}$$

3. Global sensitivity analysis of the frequency response functions

The frequency response functions given in equations (23), (24) and (25) establish the dependence of the output responses on a set of parameters representing the physical characteristics of the harvester. These parameters are regrouped in a vector $\boldsymbol{\theta}$ which is assumed to contain k independent random parameters. The output Y is determined using a deterministic model $\mathcal{M}$ which depends on the components of vector $\boldsymbol{\theta}$. In general, we assume that for any complex frequency response function H of the bimorph MFC-harvester, the output can be expressed in the following form:

$$Y = \mathcal{M}(\boldsymbol{\theta}) = |H(\omega,\boldsymbol{\theta})| \tag{26}$$

where $|.|$ is the modulus and ω is the excitation angular frequency. Even though the response Y depends on ω, the sensitivity analysis is limited to the set of parameters of vector $\boldsymbol{\theta}$.

In practice, the global sensitivity analysis is conducted by applying the following steps [28, 39]: *(a)* defining the model and its input parameters, *(b)* assigning a Probability Density Function (PDF) to each input parameter, *(c)* generating an input matrix using an appropriate random sampling method (e.g. latin hypercube sampling, Monte Carlo sampling ...), *(d)* calculating the corresponding output response vector, and *(e)* computing the appropriate sensitivity measures of each input/output relationship. In this paper, two GSA methods are applied for sensitivity analysis of the frequency response functions of an MFC harvester to variations of its physical parameters which are introduced in the following two subsections.

3.1. The elementary effects method

The elementary effects method constitutes a simple way for screening the effect on the model output of a few important input factors among many others. The fundamental idea behind this technique is given by Morris [40, 41], who introduced the concept of Elementary Effects (EEs), proposing two sensitivity measures: the *mean* and the *standard deviation* of a set of EEs for each input factor. The main goal is to determine which factors could be considered to have effects which are: *(i)* negligible (low mean, low standard deviation), *(ii)* linear and additive (high mean, low standard deviation), *(iii)* non-linear or involved in interactions with other factors (high standard deviation) [42].

A discretized approach of the input space is proposed. Each parameter θ_i is assumed to be non-dimensional and scaled to take on values in the interval $[0,1]$. Thus, these parameters are randomly selected in a k-dimensional unit hypercube. In practice, the possible input values will be restricted to an experimental design, which is a regular k-dimensional p-levels grid, where each θ_i may take a value from the set $\{0,1/(p-1),2/(p-1),\cdots,1\}$. For a given vector $\boldsymbol{\theta}$, the elementary effect of the i^{th} input parameter is defined as follows [30, 42]:

$$d_i(\boldsymbol{\theta}) = \frac{Y(\theta_i+\Delta,\boldsymbol{\theta}_{\sim i})-Y(\boldsymbol{\theta})}{\Delta} \tag{27}$$

where θ_i varies between 0 and $(1-\Delta)$; Δ is the variation size which is a predetermined multiple of $1/(p-1)$, and $\boldsymbol{\theta}_{\sim i}$ is the set of all parameters except the i^{th} parameter. The originality of the elementary effects method is based on selecting a set of r trajectories in which the parameters are changed one at a time on the design grid [43]. A trajectory enables the calculation of an elementary effect for each input parameter θ_i between two points of the trajectory ($\boldsymbol{\theta}^{(j)}$ and $\boldsymbol{\theta}^{(j+1)}$, where $j\in\{1,..,k\}$). Therefore, each trajectory requires $(k+1)$ model evaluations to calculate k elementary effects (one EE per parameter). A set of r different trajectories (with index t, where $t=1,..,r$) provides r estimates of elementary effects related to each input parameter ith, at the cost of $r\times(k+1)$ simulations.

The first measure of sensitivity is the average of the absolute values of the elementary effects which is computed for each input parameter ith:

$$\mu_i^* = \frac{1}{r}\sum_{t=1}^{r}|d_i^{*(t)}| \tag{28}$$

where d_i^* is the normalized elementary effect to the interval of variability corresponding to the parameter θ_i.

The second proposed measure is the standard deviation of the EEs σ_i, which assesses the extent of interactions and non-linear effect of each input parameter ith. This measure is defined as follows:

$$\sigma_i = \sqrt{\frac{1}{r-1}\sum_{t=1}^{r}(|d_i^{*(t)}|-\mu_i^*)^2} \tag{29}$$

3.2. Variance based sensitivity analysis

Among the large number of variance-based methods proposed for sensitivity analyses, the method based on Sobol' indices is commonly used and widely applied to characterize parameter sensitivities. This method decomposes the variance of

the model output into fractions which can be attributed to inputs or sets of inputs. The output Y in equation (26) can be orthogonally decomposed as follows [31]:

$$Y(\boldsymbol{\theta}) = \mathcal{M}_0 + \sum_{i=1}^{k} \mathcal{M}_i(\theta_i) + \sum_{i<j}^{k} \mathcal{M}_{ij}(\theta_i,\theta_j) + \cdots + \mathcal{M}_{12\cdots k}(\boldsymbol{\theta}) \tag{30}$$

where the constant $\mathcal{M}_0$ and conditional expectations $\mathcal{M}_i, \mathcal{M}_{ij}, \cdots, \mathcal{M}_{12\cdots k}$ are expressed as follows:

$$\mathcal{M}_0 = \mathbb{E}(Y) \tag{31a}$$

$$\mathcal{M}_i(\theta_i) = \mathbb{E}(Y|\theta_i) - \mathcal{M}_0 \tag{31b}$$

$$\mathcal{M}_{ij}(\theta_i,\theta_j) = \mathbb{E}(Y|\theta_i,\theta_j) - \mathcal{M}_0 - \mathcal{M}_i - \mathcal{M}_j \tag{31c}$$

...etc

This expansion is unique under the following conditions [44]:

$$\int_0^1 \mathcal{M}_{i_1\cdots i_s}(\theta_{i_1},\cdots,\theta_{i_s}) d\theta_{i_t} = 0, \quad 1 \le t \le s, \quad \{i_1,\cdots,i_s\} \subseteq \{1,\cdots,k\} \tag{32}$$

The variance of the output Y is decomposed as follows:

$$\mathrm{Var}(Y) = \sum_{i=1}^{k} D_i(Y) + \sum_{i<j}^{k} D_{ij}(Y) + \cdots + D_{12\cdots k}(Y) \tag{33}$$

where $D_i(Y) = \mathrm{Var}[\mathbb{E}(Y|\theta_i)]$, $D_{ij}(Y) = \mathrm{Var}[\mathbb{E}(Y|\theta_i,\theta_j)] - D_i(Y) - D_j(Y)$ and so on for higher order interactions. Hence, the *Sobol' indices* are obtained as follows:

$$S_i = \frac{D_i(Y)}{\mathrm{Var}(Y)}, \quad S_{ij} = \frac{D_{ij}(Y)}{\mathrm{Var}(Y)}, \quad \cdots \tag{34}$$

The important indices in practice are the main effect S_i and the total effect S_{Ti} which is defined below. Their values in most cases provide sufficient information for the sensitivity analysis of the output system to its individual input variables. The simplest approach is to estimate the first order indices (main effects) $\{S_1,\cdots,S_k\}$ and to sort these indices in descending order [30, 31]. The indices are all positive and varying between 0 and 1; the larger is an index with a value close to 1, the most significant is effect on the output.

The total sensitivity index (total effect), denoted as S_{Ti}, includes all the effects associated with the parameter θ_i and defined as the sum of all the indices associated with θ_i which corresponds to the variance of Y induced by θ_i for fixed values of other variables. Thus:

$$S_{Ti} = 1 - \frac{\mathrm{Var}[\mathbb{E}(Y|\theta_{\sim i})]}{\mathrm{Var}(Y)} \tag{35}$$

where $\theta_{\sim i}$ denotes all factors except θ_i. The condition $S_{Ti} \approx 0$ is necessary and sufficient for θ_i to be a non-influential factor. If $S_{Ti} = 0$, then θ_i can be fixed at any value within its range of uncertainty without appreciably affecting the value of the output variance $\mathrm{Var}(Y)$. Thus, the total indices can be used in setting certain parameters at fixed value.

The difference between the two Sobol' indices S_{Ti} and S_i corresponds to the interactions effect of θ_i with the other parameters which is included into S_{Ti} but not in S_i.

4. Stochastic prediction analysis and uncertainty propagation

The variability in the model parameters are transferred to the model output Y of the MFC-harvester; and influence its response distribution, which leads to the uncertainty quantification issue known as uncertainty propagation [45]. The uncertainty analysis requires the construction of a consistent stochastic model.

4.1. Prediction analysis

The stochastic model requires the assumption of a probability distribution function $p(Y|\boldsymbol{\theta})$ of the real output Y at the interest point $\boldsymbol{\theta}$ which corresponds to the model parameters vector. The expected value of the output response Y for a given vector $\boldsymbol{\theta}$ is expressed as follows:

$$\mathbb{E}[Y|\boldsymbol{\theta}] = \int Y p(Y|\boldsymbol{\theta})\, dY \tag{36}$$

The uncertainties propagation related to model parameters is incorporated into equation (36) by including the probability distribution function of the parameters, denoted as $p(\boldsymbol{\theta})$, thus:

$$\mathbb{E}[Y] = \int Y p(Y|\boldsymbol{\theta})\, p(\boldsymbol{\theta})\, dY d\boldsymbol{\theta} \tag{37}$$

This concept can be extended to define the expected value of any other performance function $f(Y)$ depending on the output Y as follows:

$$\mathbb{E}[f(Y)] = \int f(Y) p(Y|\boldsymbol{\theta})\, p(\boldsymbol{\theta})\, dY d\boldsymbol{\theta} \tag{38}$$

The variance of the real output Y is defined as follows [46]:

$$\mathrm{Var}[Y] = \int (Y p(Y|\boldsymbol{\theta}))^2 p(\boldsymbol{\theta})\, dY d\boldsymbol{\theta} - (\mathbb{E}[Y])^2 \tag{39}$$

The probabilistic integral is commonly solved via stochastic simulations, corresponding to a broad class of computational methods that are sampling-based (e.g. Monte Carlo method, Latin hypercube ...). A brief overview of the direct Monte Carlo method is presented in the next section.

4.2. Monte Carlo simulation

The most frequently technique used to compute the propagation of the parameters uncertainties through a computational model is the Monte Carlo method (MCM), originally proposed by N Metropolis and S Ulam [47]. Briefly, the uncertainty propagation problem consists in determining the probability distribution of the model output based on selected probability distributions for the uncertain input-parameters.

The MCM is used to generate K random samples of the k parameters based on a selected joint distributions stochastic model. Thus, the computational experiments are organized using $\boldsymbol{\theta}^{(j)}$ as the j^{th} row of the $K \times k$ dimensional input matrix. Based on the central limit theorem, the MCM consists in estimating the expected value of the output Y using the average of all realizations $Y(\boldsymbol{\theta}^{(j)})$ as follows [48, 49]:

$$\widehat{Y} = \frac{1}{K}\sum_{j=1}^{K} Y(\boldsymbol{\theta}^{(j)}) \tag{40}$$

Thus, $\widehat{Y}$ is the approximation of the theorical $\mathbb{E}[Y]$ obtained using the Monte Carlo method. The minimum number of required samples K can be estimated by selecting a value for the coefficient of variance δ_{MC} defined as follows [27]:

$$\delta_{MC} = \frac{1}{\sqrt{K}} \frac{\sqrt{\frac{1}{K}\sum_{j=1}^{K} Y(\boldsymbol{\theta}^{(j)})^2 - \left(\frac{1}{K}\sum_{j=1}^{K} Y(\boldsymbol{\theta}^{(j)})\right)^2}}{\frac{1}{K}\sum_{j=1}^{K} Y(\boldsymbol{\theta}^{(j)})} \tag{41}$$

It should be noted that if K approaches infinity than δ_{MC} approaches zero.

5. A numerical example

5.1. Description of the MFC harvester and settings for bounds of model parameters

Considering an MFC-harvester which consists of a cantilever beam subjected to base vibration as shown in figure 3. The harvester is composed of two laminated MFC-patches M-8514-P1 manufactured by Smart Materials [50] which are bonded together using a vacuum process. Therefore, an epoxy bonding layer is formed between the two MFC-patches. The geometrical dimensions and material properties of the harvester used in this example are given in tables 2 and 3. Moreover, the effective surface area A_e is calculated to be 0.02 mm^2 using the experimental measured capacitance of the MFC-patch; the data is adapted from Shahab and Erturk [18, 37]. In this study, the effective surface area $A_e = b_p \times u_e$, where $u_e = 5.626 \times 10^{-2}$ mm is the effective electrode width in the length direction (x-direction) and b_p is the uncertain width of the piezoceramic fiber. For the numerical simulation, the first and second modal mechanical damping ratios are set to values $\varsigma_1 = 0.02$ and $\varsigma_2 = 0.022$. The load resistance R is assumed to be mounted in parallel with the MFC-patches as shown in figure 3(c).

The selected uncertain parameters are the Young's modulus, the material densities for both the epoxy matrix and the piezoceramics fibers; in addition to the geometrical dimensions of the the RVE and the permittivity and piezoelectric constants for the PZT fibers. Table 3 lists the tolerances provided by the manufacturers for the M-8514-P1 as a percent variation from the nominal values [27, 50]. A tolerance of $\pm 20\%$ is reported for the piezoceramics electromechanical properties and $\pm 10\%$ for the Young's modulus and density of the epoxy matrix. For the geometrical dimensions of the RVE, an interval of $\pm 2.5\%$ for the length, $\pm 10\%$ for the thickness (the same thickness for the fibers and epoxy matrix) and $\pm 7\%$ for the width of both fibers and epoxy matrix are assumed. For the sensitivity analysis, all values within these bounds are assumed to have the same likelihood. Therefore, a uniform distribution is assumed for all parameters of the harvester.

5.2. Electromechanial response analysis of the MFC harverster

The validation of the MFC-harvester model is fulfilled for the frequency range from 0 to 1000 Hz by comparing the few first resonance frequencies computed by the analytical model, equation (17), to those found by experimentation as reported in [18, 37] for the same structure and for the short-circuit and open-circuit conditions. The first three natural frequencies are listed in table 4. The open-circuit natural frequencies correspond to the peaks of the resonance frequencies of the displacement response of the harvester when the load resistance tends infinity. In practice, these can be determined by connecting a very large electrical resistance so that any further increase of load resistance does not change the resonance frequency of the tip displacement response. In that case, the peaks of the displacement response match the open-circuit resonance frequencies. Since it is a forced system, the verification of the response amplitude is essential for model validation. For that reason, the experimental data from the research paper [18] are added to figure 4(a). We can notice that the natural frequencies for the open-circuit condition are higher than those obtained in the short-circuit case due to the electromechanical coupling effects and the added stiffness in the open-circuit condition. The short-circuit natural frequencies found analytically are thus in good agreement for the first and the second mode with errors not exceeding 3%. These results support the validity of the analytical MFC-harvester model and allow for pursuing the sensitivity analysis of the responses.

Figure 4 shows the voltage output and the tip displacement FRFs (per base acceleration) of the MFC-harvester for a frequency range $(20\ \text{Hz}, 80\ \text{Hz})$ in the vicinity of the first mode which are obtained using equations (23) and (24). The values of the electrical load resistance are chosen similar to those used in the experimental investigation on the same harvester reported in [37] so that a computed output can be compared to their measured counterparts. As can be seen from figure 4(a), the voltage amplitude increases with increasing electrical load resistance for all excitation frequencies. Furthermore, increasing the resistance, the first natural frequency moves slightly from the short circuit to the open circuit resonance frequency.

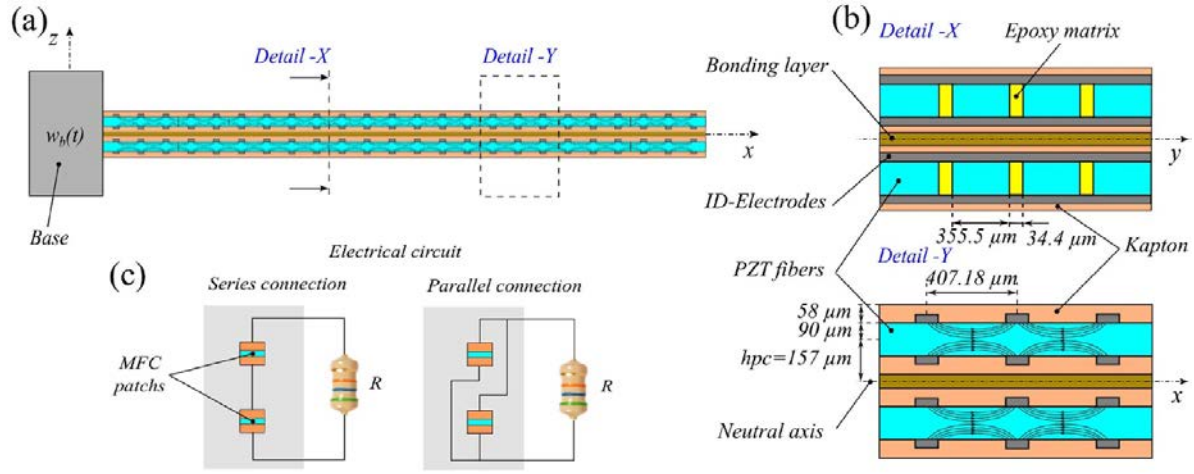

Figure 3. Two-dimensional view of the bimorph MFC-harvester with geometrical specifications and the two electrical circuit configurations: (a) the MFC-harvester with base excitation, (b) details X and Y, (c) the series and parallel connections of the load resistance.

Table 2. Geometrical and material properties of the MFC-patch Smart Material M-8514-P1.

Parameters	Descriptions	Values	Units
L	Active length	75.5	mm
b	Active width	14	mm
E_k	Young's modulus of the Kapton	2.8	GPa
E_e	Young's modulus of the electrode copper	117.2	GPa
c_{33}^E	Overall Young's modulus for one patch	31.1	GPa
e_{33}	Overall piezoelectric constant for one patch	13.6	C m^{-2}
M	Number of PZT fibers along the y-direction	36	–
Nth	Number of electrode pairs	185	–
ν_1	PZT fibers volume fraction	0.9	–
ν_2	Electrodes copper volume fraction	0.24	–

Table 3. Bounds for the uniform PDF distribution associated to the electromechanical parameters of the RVE in figure 2; bounds are expressed in terms of the nominal values [27, 50, 51].

Parameters	Nominal values	Units	Bounds
$\overline{c}_{33,p}^E = E_p$	48.3	GPa	±20%
$\overline{c}_{33,m}^E = E_m$	3.1	GPa	±10%
ρ_p	7750	kg m^{-3}	±20%
ρ_m	1100	kg m^{-3}	±10%
$\overline{\epsilon}_{33,p}$	1850×8.854	pF m^{-1}	±20%
$\overline{\epsilon}_{33,m}$	4.25×8.854	pF m^{-1}	±10%
$\overline{d}_{33,p}$	440	pm V^{-1}	±20%
$L_e = L_{pm}$	407.18	μm	±2.5%
h_{pm}	180	μm	±10%
b_p	355.5	μm	±7%
b_m	34.4	μm	±7%

For a given load resistance, the maximum voltage output is obtained at the resonance frequency of the fundamental vibration mode. Moreover, for every excitation frequency, the maximum voltage output is obtained when the system is close to the open circuit condition. Figure 4(b) shows the resistive shunt damping effect on both natural frequency shift and vibration amplitude attenuation at the tip of the harvester. By increasing the load resistance, the electromechanical system moves from the short-circuit to the open-circuit conditions. Furthermore, the peak vibration amplitude of 4 317.2 μm g^{-1} for a 1 kΩ resistance at 47.9 Hz is attenuated to a peak amplitude of 4 042.8 μm g^{-1} for a 909.1 KΩ load resistance at 48.3 Hz, which means an increased damping effect by a factor of about 1.07. Unlike viscous damping, the resistive shunt damping shifts the frequency of peak vibration amplitude to higher values. Increasing the load resistance, the peak vibration amplitude is reduced to a minimum and then increases back up to the open-circuit condition. Physically, the stiffness of the piezoceramic fibers of the MFC patches increases from the constant electric field value to the constant electric displacement value and without overall energy dissipation. Since the maximum of the voltage and tip displacement FRFs for a given load resistance does not occur at the same frequency, it should be pointed out that the resonance frequencies for these output FRFs are slightly different.

The output voltage and the vibration response at the tip of the MFC-harvester are further analyzed for the excitation at the short- and open-circuit resonance frequencies of the first fundamental vibration mode with variation of the external load resistance as shown in figure 5. It is important to note that the peak FRF varies monotonically for the voltage FRFs in short- and open-circuit conditions in contrast to the tip displacement FRF. Figure 5(a) shows that the peak voltage increases for

Table 4. The first three natural frequencies for the short circuit and open circuit conditions computed from the current analytical model (Anal.) and the experimental study (Exp.) of [18, 37].

Mode (r)	f_r^{sc} (Anal.)	f_r^{sc} (Exp.)	Error (%)	f_r^{oc} (Anal.)	f_r^{oc} (Exp.)	Error (%)
1	47.91	47.9	0.02	48.60	48.5	0.2
2	300.23	309.8	3	300.9	–*	–*
3	840.66	–*	–*	846.10	–*	–*

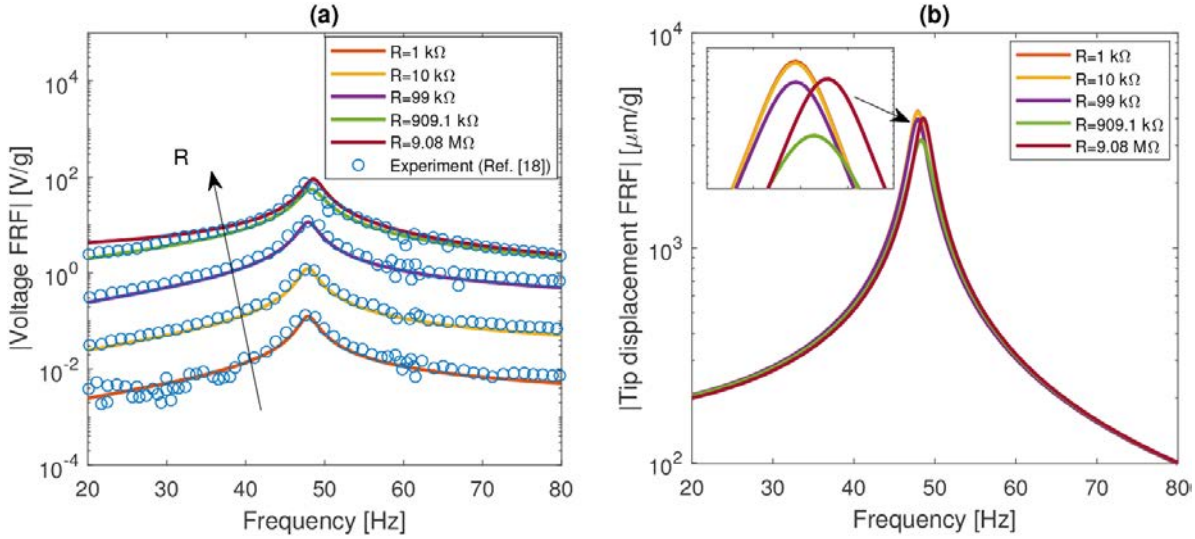

Figure 4. The modulus output FRFs of the bimorph MFC-harvester versus the frequency excitation for frequencies in the vicinity of the first vibration mode: (a) voltage FRF (b) tip displacement FRF.

low resistance values at these two particular excitation frequencies with approximately the same slope on a logarithmic scale for both x and y axis (see the enlarged view). For these low resistances, the voltage output at the short circuit resonance frequency is greater than that of the closed-circuit resonance frequency. The two curves intersect at a resistance of approximately 0.83 MΩ . For resistances greater than that of the intersection point, the voltage at the open circuit resonance frequency is slightly greater. Considering the vibration responses shown in figure 5(b), the vibration amplitude at the short circuit excitation frequency 47.9 Hz decreases from 4 320.3 μm g^{-1} for a resistance of 100 Ω to 3042 μm g^{-1} for a resistance of 1 MΩ . Further increase of the load resistance up to 100 MΩ at this excitation frequency, amplifies slightly the vibration amplitude, to reach 3493, 7 μm g^{-1}. Whereas the vibration amplitude at the open circuit excitation frequency of 48.6 Hz decreases slightly from 3 462.1 μm g^{-1} for a resistance of 100 Ω to 3 006.3 μm g^{-1} for about a resistance of 0.5 MΩ then it is strongly amplified as the load resistance is further increased to reach an amplitude of 4 226.2 μm g^{-1}.

Moreover, it is also useful to note that these resistance loads of maximum vibration attenuation are not those of maximum harvested voltage. Thus, shifting the excitation frequency of the harvester from 47.9 Hz to 48.6 Hz (i.e. from the short- to the open-circuit excitation frequencies) induces an attenuation of the tip displacement per base acceleration amplitude by 19.86% in the short-circuit condition and an amplification by 20.97% in the open circuit condition at 100 MΩ .

5.3. Global sensitivity and uncertainty analysis of the output voltage

Considering the application of the GSA on the output voltage of the bimorph MFC-harvester, the Morris method is firstly applied with $r = 30$ elementary effects for each of the $k = 11$ parameters listed in table 3. Thus, the numerical computation cost is $r \times (k+1) = 360$ model evaluations (simulations) for a fixed excitation frequency and external load resistance. For a given parameter θ_i, if the r estimates of elementary effect have the same sign, that means that this parameter has a monotonic effect on the output response, increasing or decreasing, depending on the sign of the elementary effect. Secondly, the Sobol indices are computed using equations (34) and (35). Monte Carlo estimations of the response are then computed by employing $1000 \times (k+2) = 13000$ samples. The Morris elementary effects and the Sobol indices are computed for a set of excitation frequencies in the vicinity of the first fundamental natural frequency of the MFC-harvester for a small load resistance value (i.e. a nearly short-circuit condition) then for a high resistance which approximates the open-circuit condition.

5.3.1. Global sensitivity analysis using Morris elementary effects. Figure 6 shows the absolute average μ^* and the standard deviation σ of the elementary effects corresponding to the uncertainty on the 11 physical parameters of the bimorph MFC energy harvester for the output voltage FRF at a selected set of excitation frequencies in the vicinity of the first natural

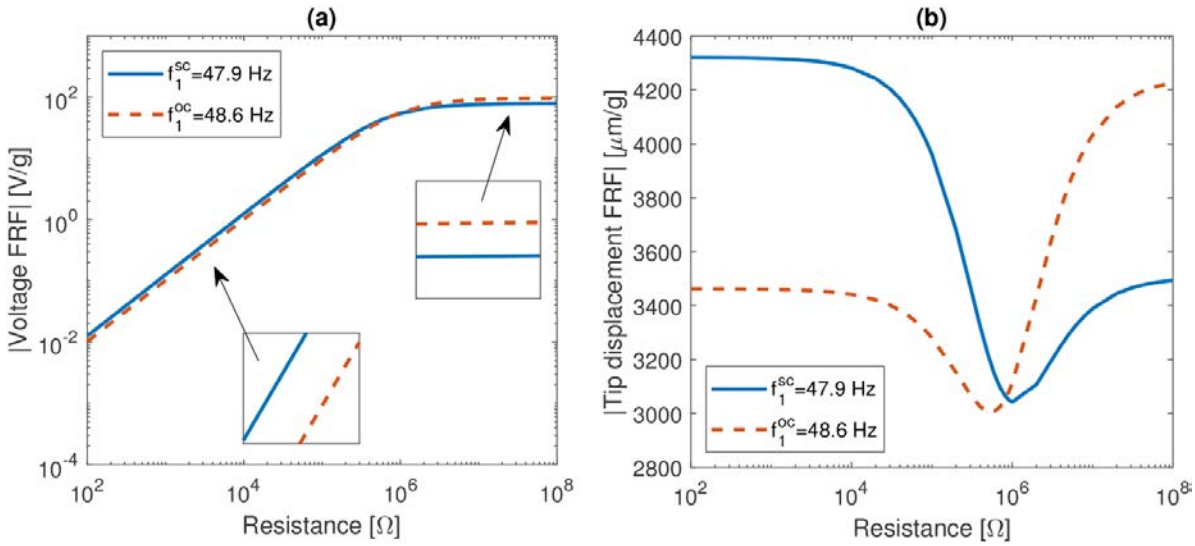

Figure 5. Variation of the modulus of the voltage and the tip displacement FRFs relative to the base excitation with the electrical load resistance for excitations at the short-circuit and the open-circuit resonance frequencies of the first vibration mode.

frequency. The excitation frequencies are varied from 35 Hz to 60 Hz by a step of 5 Hz . The MFC-harvester has a 100 Ω load resistance mounted in parallel connection between the interdigitated electrodes. For an easier analysis of the results, the parameters are presented in a decreasing order of their importance. Figure 6(a) shows that the hierarchical influence of the input parameters on the output voltage is unchangeable and independent of the excitation frequency. The density of the piezoelectric fibers ρ_p, the elastic modulus of the piezoceramics fibers E_p, the length L_{pm} and the thickness h_{pm} of the RVE have the highest values of the EEs indicators whereas the permittivity constant of both fibers and matrix have the lowest values. These results confirm other research findings of Aloui *et al* [28] and Ruiz *et al* [27] which indicate that the hierarchical influence of the input physical parameters is unchangeable and independent of the excitation frequency. Therefore, a sensitivity analysis of the MFC-harvester at a single excitation frequency is sufficient to identify the parameters with the highest effect on the output. Figure 6(b) shows the standard deviation of the EEs of the uncertain parameters considered above. The density of the piezoelectric fibers ρ_p, the thickness h_{pm} and the length L_{pm} of the RVE and the elastic modulus of the piezoceramics fibers E_p have the highest values. This means that these parameters are strongly influenced by the non-linear effects and interactions with others parameters. In addition, it should be noted that the variation of these parameters affects the responses of the harvester through the modal damping ratio ζ_r and the electromechanical coupling term θ_r. The damping ratio given in equation (20) depends on the internal strain damping and the external air viscous damping in addition to the geometrical and material properties of the harvester and the considered natural frequency. The increase of damping ratio reduces the peak of the voltage response at the considered natural frequency and increases the bandwidth response so that more tolerance is allowed for the variation of the excitation frequency in the vicinity of the natural frequency. On the other hand, the modal electromechanical coupling term given in equation (21) depends on geometrical, material, and density of fibers for a given vibration mode. For a given choice of fibers, this term can be increased by increasing fiber density M, reducing the interdigitated electrodes and the distance of the fiber from the neutral axis. The variation of the electromechanical coupling term, for a given load resistance, induces a variation in the electromechanical stiffness that affects the overall rigidity of the harvester. So that, this term impacts the resonance frequency and affects the output voltage amplitude.

Figure 7 shows the scatter graph of the Morris measures (μ^*, σ) of the voltage FRF for the eleven uncertain parameters of the electromechanical and geometrical characteristics given in table 3 for the short circuit condition and for an electrical load resistance $R = 100\ \Omega$ and excitation frequency equal to 50 Hz . The bounds of the boxes correspond to a confidence interval of 95%. The figure shows that the sensitivity measures of the absolute mean and standard deviation of the piezoelectric density ρ_p, the elastic modulus of the fibers E_p, the length L_{pm} and the thickness h_{pm} of the RVE are relatively significant compared to those of the piezoelectric constant $d_{33,p}$, permittivity constant $\varepsilon_{33,p}$ and other geometrical dimensions for both piezoceramic fibers and epoxy matrix. Therefore, the density and elastic modulus of piezceramic fibers are the most important parameters that affect the output voltage FRF in terms of material properties, as well as the length and the thickness of the RVE for the geometrical characteristics. Furthermore, the absolute mean and the standard deviation of the EEs are of the same order of values. This shows that this group of parameters are also strongly influenced by the non-linear effect and interactions with others parameters.

Now, considering the sensitivity analysis for a nearly open circuit condition simulated by using a load resistance $R = 9.08\ \text{M}\Omega$ for electrical energy dissipation. Figure 8 shows

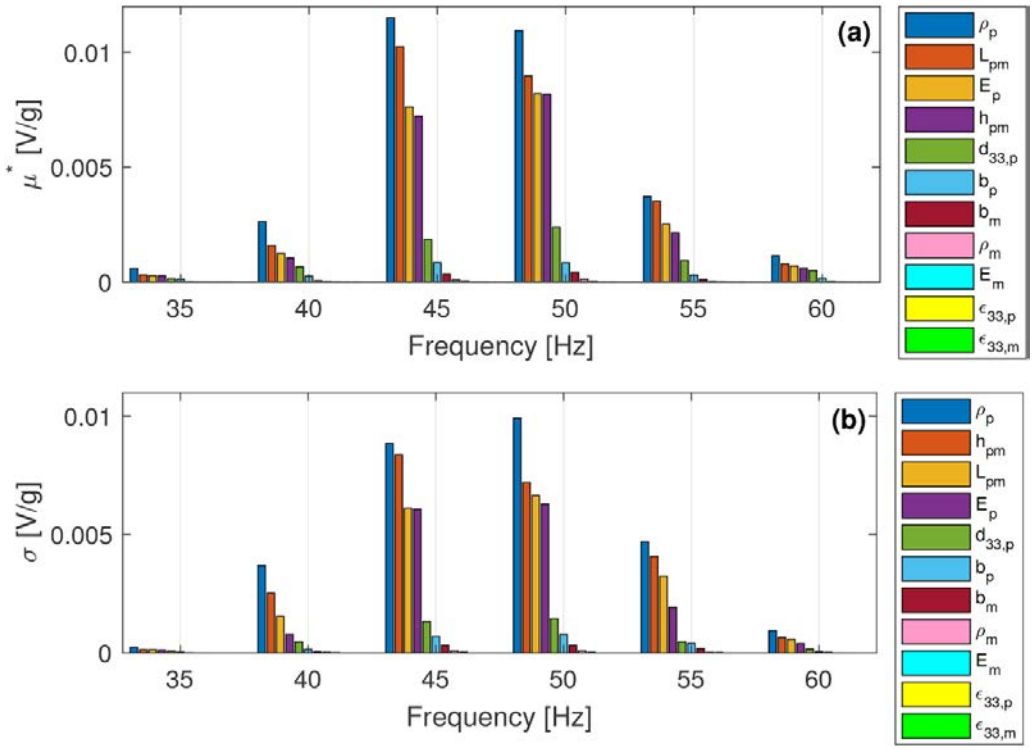

Figure 6. EEs measures for the voltage FRF of the bimorph MFC-harvester for a load resistance $R = 100\ \Omega$ at excitation frequencies in the vicinity of the first natural frequency (a) the mean and (b) the standard deviation.

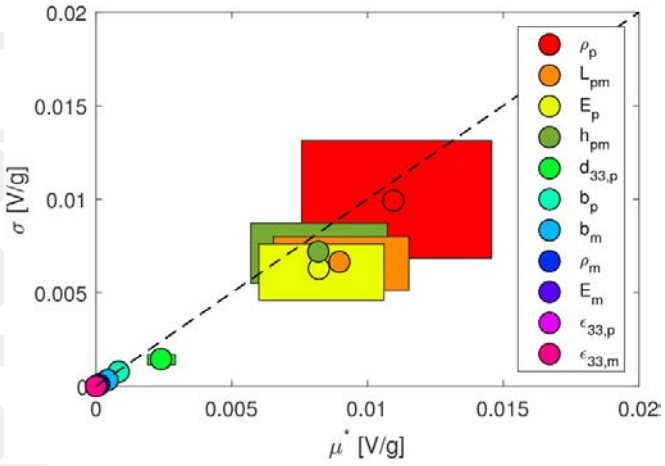

Figure 7. Scatter graph in the (μ^*, σ) plane of the modulus of voltage FRF of the MFC-harvester for an excitation frequency $f = 50$ Hz with boxes defining the limits of the 95% confidence intervals for the nearly short-circuit condition.

the absolute mean μ^* and the standard deviation σ of the elementary effects for the voltage output at a set of excitation frequencies in the vicinity of the first fundamental natural frequency. The figure reveals that the elementary effects sensitivity measures follow the same order of significance for all considered excitation frequencies. This confirms that the order of importance of the effect of parameters on the voltage output is the same independently of the excitation frequency. Furthermore, one can notice that the influence of the permittivity constant of the PZT fibers becomes more significant compared to the short-circuit condition. Thus, the influence order of the parameters on the output changes from the short to the open circuit conditions. Nevertheless, the density ρ_p, the elastic modulus E_p of the PZT fibers, the length L_{pm} and the thickness h_{pm} remain the parameters with the highest effect on the voltage output in addition to the piezoelectric coupling constant $d_{33,p}$ and the permittivity constant $\varepsilon_{33,p}$.

5.3.2. Global sensitivity analysis using the variance method. Considering the sensitivity analysis using the variance method, figure 9 presents the Sobol' indices (S_i, S_{Ti}) of the voltage FRF for the parameters listed in table 3, for a load resistance $R = 100\ \Omega$ (i.e. a nearly short circuit condition) and a base excitation frequency of 50 Hz . The figure reveals that the sensitivity measures of the main effects (S_i) and those of the total effects (S_{Ti}) are particularly significant for the density ρ_p and the elastic modulus E_p of the piezoceramics fibers, as well as the length L_{pm} and the thickness h_{pm} of the RVE compared to other uncertain parameters. Thus, the piezoceramics fiber density and elastic modulus are the most influential parameters with the highest impact on the output voltage of the MFC-harvester. Furthermore, the length and the thickness of the RVE are the most influential geometrical characteristics. These findings confirm the global sensitivity analysis using the screening method of Morris described above. Both GSA methods lead to the same conclusion and provide more confidence on the results of the sensitivity analysis.

Table 5 presents the absolute mean μ_i^* and the standard deviation σ_i of the elementary effects and the main effect S_i

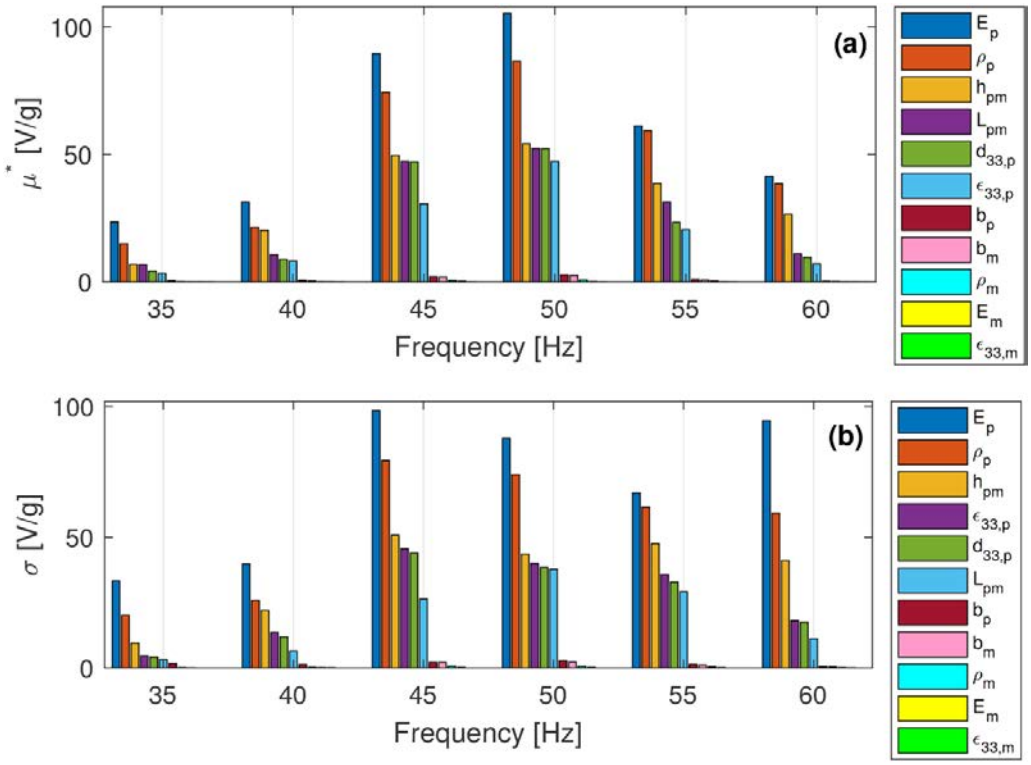

Figure 8. EEs measures for the voltage FRF of the bimorph MFC-harvester for a load resistance $R = 9.08$ MΩ at excitation frequencies in the vicinity of the first natural frequency (a) the mean and (b) the standard deviation.

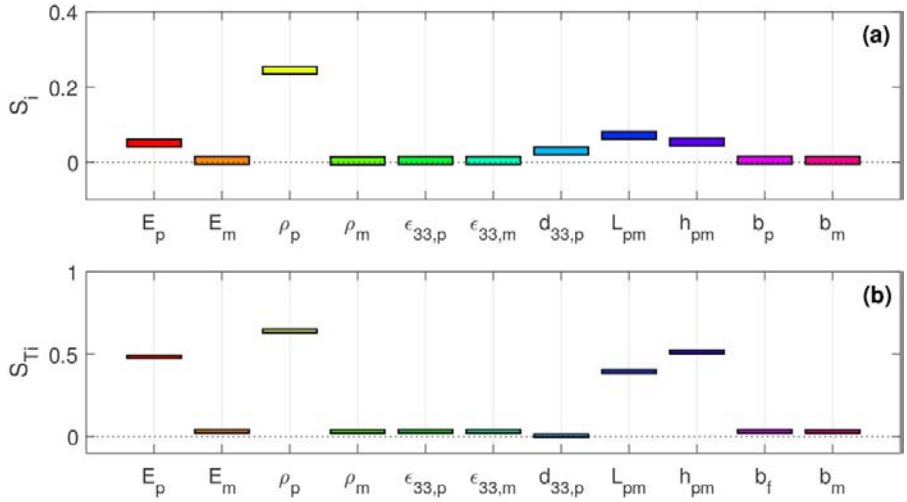

Figure 9. Sobol's indices for the modulus voltage FRF of the MFC-harvester for an excitation frequency $f = 50$ Hz and a nearly short-circuit condition simulated by using a load resistance $R = 100$ Ω.

and the total effect S_{Ti} for the eleven uncertain physical characteristics of the MFC-harvester for the case of a nearly open circuit condition depicted by a load resistance $R = 9.08$ M Ω and for an excitation frequency of 50 Hz . One can clearly notice that the PZT fiber density ρ_p and its elastic modulus E_p remain the major contributors for the uncertainty of the voltage FRF. The permittivity constant of the piezoelectric fibers becomes more significant compared to the epoxy matrix characteristics which have negligible effect on the harvester voltage output in both short and open circuit. Furthermore, the width of both PZT fibers and epoxy matrix have negligible effect on the variability of the output. The two GSA methods are in agreement about the parameters which have the most influence on the response. These parameters are identified based on the average μ_i^* of the EEs method and the main effect S_i (first order sensitivity of the variance method). The total effect sensitivity index S_{Ti} shows a strong interaction for these parameters. In addition, the widths of both fibers and matrix and the epoxy properties retain their order of importance compared to the short-circuit condition; however,

Table 5. Morris measures (μ^*, σ) and Sobol indices (S_i, S_{Ti}) of the modulus voltage FRF of the MFC-harvester for an excitation frequency $f = 50$ Hz for the open-circuit condition.

	μ_i^*	σ_i	S_i	S_{Ti}
E_p	104.676	87.191	0.160	0.708
E_m	0.239	0.268	0.021	0.027
ρ_p	87,258	73.671	0.201	0.826
ρ_m	0.817	0.636	0.022	0.030
$\overline{\epsilon}_{33,p}$	46.831	39.697	0.121	0.087
$\overline{\epsilon}_{33,m}$	0.008	0.011	0.021	0.027
$\overline{d}_{33,p}$	51.650	37.781	0.117	0.094
L_{pm}	52.310	37.839	0.173	0.491
h_{pm}	54.051	43.428	0.185	0.512
b_p	2.776	2.754	0.023	0.034
b_m	2.510	2.214	0.020	0.031

the permittivity constant of PZT fibers becomes more significant with small interaction effect according to the total effect.

Although the two GSA methods used are strategically different, they give very close and agreeable results. The elementary effects method is only semi-quantitative which is not a favorable feature of the method. However, the focus of the sensitivity analysis of this paper is limited to finding the order of importance of the parameters. For the variance-based sensitivity method, we have found that the numerical stability of the Sobol' indices in this case study is quite low which means that the results for a given sample size showed high variance. This effect did not diminish with increasing sample size.

5.3.3. Uncertainty analysis using Monte Carlo simulations. In the following, the uncertainty analysis applied using Monte Carlo simulations is presented. The analysis consists in quantifying the uncertainty of the model output due to uncertain input parameters which are uniformly distributed within ranges given in table 3. Figure 10 shows the density histogram and the normal probability plot for the voltage FRF amplitude, at 20 Hz and 30 Hz excitation frequencies and 100 Ω load resistance, according to the model parameters uncertainties. The voltage output of the stochastic harvester model is evaluated 13000 times using independent realizations generated with the Monte Carlo method. The voltage output followed an approximately Gaussian probability density function even though it lacks symmetry. Despite the high computational cost due to the Monte Carlo simulations, the simulation results provide a mean for understanding the influence of the input uncertainties on the voltage produced by the MFC energy harvester.

Figure 11 shows the nominal voltage FRF and the expected FRF relative to the stochastic model of the MFC-harvester for the short and open circuit conditions and for a frequency range (20 Hz, 80 Hz) . The 95% confidence interval is shown as a shaded band around the curve of the expected FRF. The parameters of low effect on the output voltage have been maintained constant in the simulation. Figure 11(a) presents the uncertainty propagation in the short circuit-condition, in which only the density ρ_p, the elastic modulus E_p of the PZT fibers, the length L_{pm} and the thickness h_{pm} of the RVE and $d_{33,p}$ of the PZT fibers are considered as uncertain parameters. Whereas, figure 11(b) presents the uncertainty quantification in the open circuit-condition, where the considered uncertain parameters are the same as those of the short-circuit case but adding the permittivity $\varepsilon_{33,p}$ of the PZT fibers. The fixed parameters are the properties of the epoxy matrix (E_m, ρ_m), the width of both fibers and matrix (b_p, b_m) and the permittivity constant of the epoxy matrix $\varepsilon_{33,m}$. It can be observed in both figures 11(a) and (b) that the nominal voltage FRF amplitude may exceed the expected FRF or even the upper limit of 95% confidence interval in the vicinity of the resonance frequency. The first interesting observation is that the probability of obtaining the nominal peak amplitude is less than 5%. Another research study carried out on monolithic piezoelectric harvester confirms this result [27]. In addition, away from the resonant frequency, the nominal FRF underestimates the expected amplitude of the FRF. These results have important implications for the design process of the MFC-harvester. Since the vibration source is frequently a narrow band process, there is at least 95% probability that the actual output voltage is lower than the nominal voltage output due to the uncertainty of the input parameters.

5.4. Global sensitivity analysis of the output power

This section presents the global sensitivity analysis of the power FRF of the bimorph MFC-harvester for the uncertain physical parameters. The power is defined as a function of the output voltage $P(t) = \dfrac{v(t)^2}{R}$, and its FRF is given in equation (25). Indeed, the goal is to check if the global sensitivity analysis of the power output leads to the same conclusions as the global sensitivity of the voltage output. The GSA of the power output is thus performed using only the Morris method which is chosen because of its low computational cost.

Figure 12 shows the scatter graph of the Morris measures (μ^*, σ) for the power FRF, with a confidence interval of 95% presented by the boxes, for the eleven uncertain parameters for the short-circuit and open-circuit conditions. Figure 12(a) shows that the absolute mean and standard deviation of the EEs of the piezoelectric density ρ_p, the elastic modulus of the fibers E_p, the length L_{pm} and the thickness h_{pm} of the RVE are relatively important compared to those of the piezoelectric constant $d_{33,p}$, permittivity constant $\varepsilon_{33,p}$ and other geometrical dimensions for both piezoceramic fibers and epoxy matrix. In figure 12(b), the results correspond to the open-circuit condition which is simulated using a high load resistance. One can notice that the importance order of the parameters effect on the output power changes compared to the short-circuit conditions. Indeed, the permittivity constant of the PZT fibers $\varepsilon_{33,p}$ becomes more significant. However, the elastic modulus E_p, the density ρ_p of the PZT fibers, the length L_{pm} and the thickness h_{pm} remain the parameters with the highest impact on the output power in addition to the piezoelectric coupling constant $d_{33,p}$ and the permittivity constant $\varepsilon_{33,p}$. These results confirm

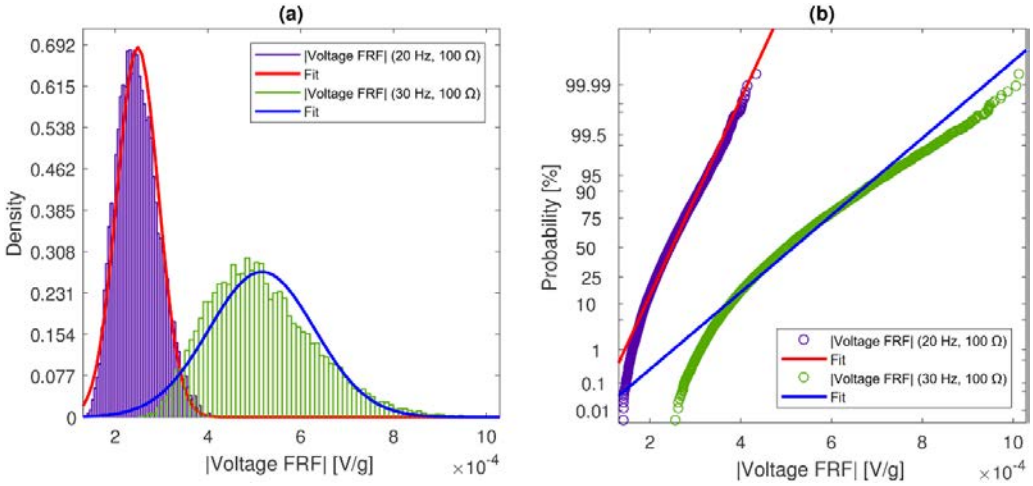

Figure 10. (a) the density of the voltage output (b) normal probability plot for of the voltage output.

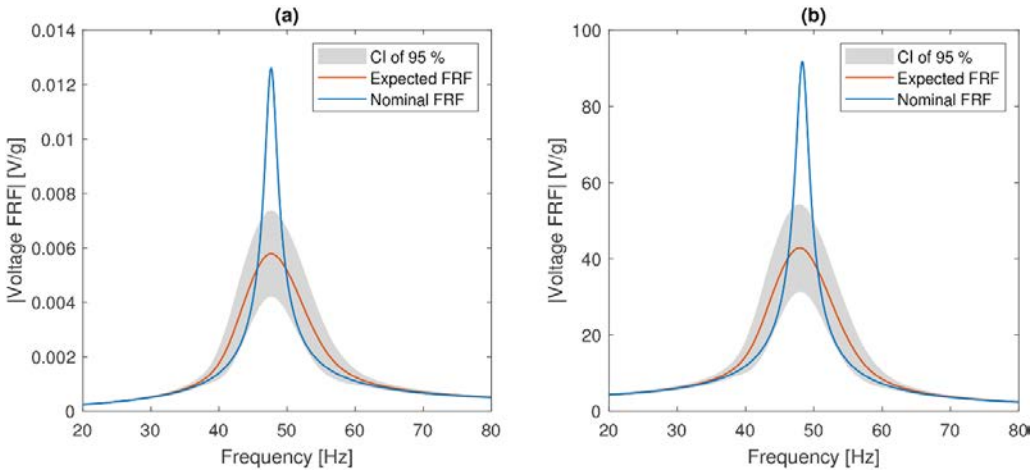

Figure 11. The modulus of the voltage FRF of the MFC-harvester for nominal configuration, expected prediction, and its 95% confidence interval: (a) short-circuit and (b) open-circuit condition.

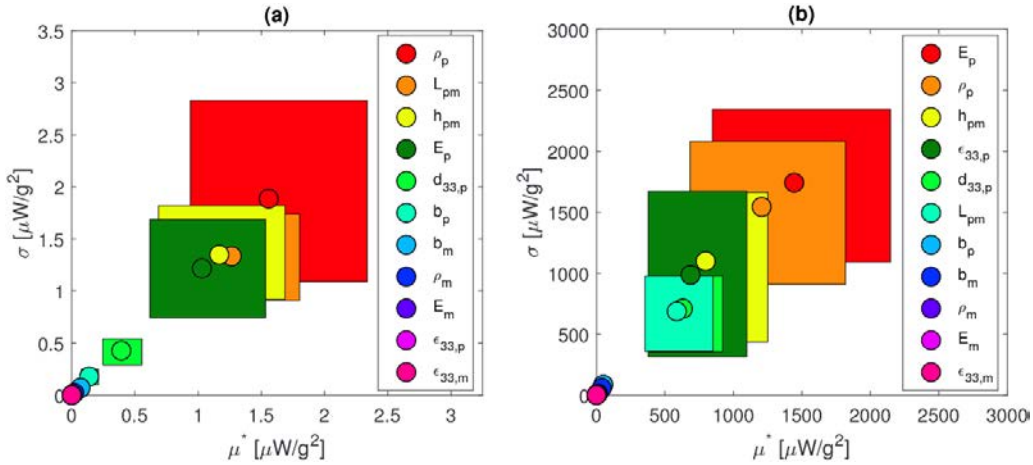

Figure 12. (μ^*, σ) Scatter graph of the modulus power FRF of the MFC-harvester for an excitation frequency $f = 50$ Hz with 95% confidence intervals for: (a) the short-circuit condition with $R = 100\ \Omega$ and (b) the open-circuit condition with $R = 9.08\ \text{M}\Omega$.

the *a priori* hypothesis that the voltage and the electrical power are similarly sensitive to the uncertain physical parameters.

6. Conclusions

In this paper, the distributed-parameters coupled electromechanical problem is firstly introduced for a bimorph MFC-harvester. The equivalent electroelastic properties of the MFC-patch are calculated using the rule of mixture for a representative volume element. Afterwards, the frequency response functions relative to the base motion of the harvester are determined and used as the deterministic performance predictors for both tip displacement amplitude and voltage output. The global sensitivity analysis is performed for the voltage FRF of the MFC-harvester using the screening method of Morris based on the elementary effects measures and Sobol' indices based on the variance decomposition to study the effect of the variability of the material properties and geometrical dimensions of the MFC-patches on the voltage output of the harvester. The Morris method correctly screened the most and least sensitive parameters among the eleven selected parameters and showed that the piezoelectric density ρ_p, the elastic modulus E_p, the length L_{pm} and the thickness h_{pm} are relatively influential compared to others parameters. Furthermore, a large output sensitivity does not necessarily match significant uncertainties because the input uncertainty might be very small in a real system; e.g. the case of the RVE length L_{pm} in this study. These results are confirmed by the variance method using Sobol' indices. The results obtained from the two methods are in agreement in ranking the parameters according to their influence on the voltage output. Furthermore, it has been shown that the order of importance of the parameters can change from the short-circuit to the open-circuit condition. For instance, some parameters have gained more influence on the output in the open-circuit condition; e.g. the permittivity constant of the PZT fibers. Monte Carlo simulations were performed to evaluate the effect of parametric uncertainties on the voltage output of the MFC-harvester using a stochastic model and to estimate the overall output uncertainty. The voltage output bounds are determined for a confidence interval of 95% in the short- and the open-circuit conditions. The research reported in this paper provide valuable information about the parameters that have a significant impact on the voltage and the power outputs of a bimorph MFC-harvester and which should be used in priority by manufacturers to improve their MFC-patch design.

ORCID iD

Rabie Aloui https://orcid.org/0000-0002-8827-0069

References

[1] Kamila S 2013 Introduction, classification and applications of smart materials: An overview *American J. Appl. Sci.* **10** 876–80

[2] Aloui R, Larbi W and Chouchane M 2018 Finite element modeling and analysis of a bimorph piezoelectric energy harvester *Design and Modeling of Mechanical Systems—III* eds Haddar M, Chaari F, Benamara A, Chouchane M, Karra C and Aifaoui N (Cham: Springer Int. Publishing) (https://doi.org/10.1007/978-3-319-66697-6_118)

[3] Pereira da Silva L, Larbi W and Deü J-F 2015 Topology optimization of shunted piezoelectric elements for structural vibration reduction *J. Intell. Mater. Syst. Struct.* **26** 1219–35

[4] Larbi W, Deü J-F and Ohayon R 2012 Finite element formulation of smart piezoelectric composite plates coupled with acoustic fluid *Compos. Struct.* **94** 501–9

[5] Larbi W, Deü J-F 2018 Reduced order finite element formulations for vibration reduction using piezoelectric shunt damping *Appl. Acoustics* **147** 111–20

[6] De Marqui Junior C, Erturk A and Inman D J 2009 An electromechanical finite element model for piezoelectric energy harvester plates *J. Sound Vib.* **327** 9–25

[7] Breitbach E J 2002 *13th Int. Conf. on Adaptive Structures and Technologies* CRC Press 2003 1st edn

[8] High J R and Wilkie W K 2003 *Method of Fabricating Nasa-Standard Macro- Fiber Composite Piezoelectric Actuators*

[9] Williams R B, Grimsley B W, Inman D J and Wilkie W K 2002 *Manufacturing and Mechanics-Based Characterization of Macro Fiber Composite Actuators inAdaptive Structures and Materials Systems* (New Orleans, Louisiana, USA: ASME) vol 2002 pp 79–89

[10] Bent A A and Hagood N W 1997 Piezoelectric fiber composites with interdigitated electrodes *J. Intell. Mater. Syst. Struct.* **8** 903–19

[11] Berger H, Kari S, Gabbert U, Rodriguez-Ramos R, Bravo-Castillero J, Guinovart-Diaz R, Sabina F J and Maugin G A 2006 Unit cell models of piezoelectric fiber composites for numerical and analytical calculation of effective properties *Smart Mater. Struct.* **15** 451–8

[12] Deraemaeker A and Nasser H 2010 Numerical evaluation of the equivalent properties of macro fiber composite (MFC) transducers using periodic homogenization *Int. J. Solids Struct.* **47** 3272–85

[13] Trindade M A and Benjeddou A 2016 Finite element characterisation of multilayer d31 piezoelectric macro-fibre composites *Smart composites and composite structures In honour of the 70th anniversary of Professor Carlos Alberto Mota Soares* vol 151 pp 47–57

[14] Erturk A, Bilgen O, Fontenille M and Inman D J 2008 Piezoelectric energy harvesting from macro-fiber composites with an application to morphing-wing aircrafts *Proc. of the 19th Int. Conf. on Adaptive Structures and Technologies, Ascona, Switzerland, Oct, Citeseer* pp 6–9

[15] Jeong Song H, Choi Y-T, Wereley N M and Purekar A S 2010 Energy Harvesting Devices Using Macro-fiber Composite Materials *J. Intell. Mater. Syst. Struct.* **21** 647–58

[16] Song H J, Choi Y-T, Wereley N M and Purekar A 2014 Comparison of monolithic and composite piezoelectric material–based energy harvesting devices *J. Intell. Mater. Syst. Struct.* **25** 1825–37

[17] Bilgen O, Erturk A and Inman D J 2010 Analytical and Experimental Characterization of Macro-Fiber Composite Actuated Thin Clamped-Free Unimorph Benders *Journal of Vibration and Acoustics* **132** 051005

[18] Shahab S and Erturk A 2017 Coupling of experimentally validated electroelastic dynamics and mixing rules formulation for macro-fiber composite piezoelectric structures *J. Intell. Mater. Syst. Struct.* **28** 1575–88

[19] Sharp R and Brooks P 1988 Sensitivities of frequency response functions of linear dynamic systems to variations in design parameter values *J. Sound Vib.* **126** 167–72

[20] Ng T H and Liao W H 2005 Sensitivity analysis and energy harvesting for a self-powered piezoelectric sensor *J. Intell. Mater. Syst. Struct.* **16** 785–97

[21] de Lima A M G, Stoppa M H, Rade D A and Steffen Jr V 2006 Sensitivity analysis of viscoelastic structures *Shock Vibration* **13** 545–58

[22] Chouchane M, Guedria N and Smaoui H 2007 Eigensensitivity computation of asymmetric damped systems using an algebraic approach *Mech. Syst. Signal Process.* **21** 2761–76

[23] Lima A d, Faria A and Rade D 2010 Sensitivity analysis of frequency response functions of composite sandwich plates containing viscoelastic layers *Compos. Struct.* **92** 364–76

[24] Lasecka Plura M and Lewandowski R 2014 Design sensitivity analysis of frequency response functions and steady state response for structures with viscoelastic dampers *Vibrations Phys. Syst.* **26** 129–36

[25] Aloui R, Larbi W and Chouchane M 2019 Sensitivity analysis of frequency response functions for load resistance of piezoelectric energy harvesters *Advances in Acoustics and Vibration II* eds. Fakhfakh T, Karra C, Bouaziz S, Chaari F and Haddar M (Cham: Springer Int. Publishing) (https://doi.org/10.1007/978-3-319-94616-0_14)

[26] Iooss B and Lemaître P 2015 A review on global sensitivity analysis methods *Uncertainty Management in Simulation-Optimization of Complex Systems: Algorithms and Applications* Eds. Dellino G and Meloni C (US, Boston, MA: Springer) (https://doi.org/10.1007/978-1-4899-7547-8_5)

[27] Ruiz R O and Meruane V 2017 Uncertainties propagation and global sensitivity analysis of the frequency response function of piezoelectric energy harvesters *Smart Mater. Struct.* **26** 065003

[28] Aloui R, Larbi W and Chouchane M 2019 Global sensitivity analysis of piezoelectric energy harvesters *Composite Structures* **228** 111317

[29] Kucherenko S, Rodriguez-Fernandez M, Pantelides C and Shah N 2009 Monte Carlo evaluation of derivative-based global sensitivity measures *Reliability Eng. Syst. Safety* **94** 1135–48

[30] Saltelli A ed 2008 *Global Sensitivity Analysis: the Primer* (Chichester: Wiley) (https://doi.org/10.1002/9780470725184)

[31] Saltelli A, Annoni P, Azzini I, Campolongo F, Ratto M and Tarantola S 2010 Variance based sensitivity analysis of model output design and estimator for the total sensitivity index *Computer Phys. Commun.* **181** 259–70

[32] Erturk A and Inman D J 2008 A Distributed Parameter Electromechanical Model for Cantilevered Piezoelectric Energy Harvesters *J. Vibration Acoustics* **130** 041002

[33] Erturk A and Inman D J 2011 *Piezoelectric Energy Harvesting* (Chichester: Wiley) oCLC: ocn687714431

[34] Sun W, Liu Y, Li H and Pan D 012010 Determination of the response distributions of cantilever beam under sinusoidal base excitation *Journal of Physics: Conf. Series* **448** 012010

[35] Tan D, Yavarow P and Erturk A Nonlinear elastodynamics of piezoelectric macro-fiber composites with interdigitated electrodes for resonant actuation *Compos. Struct.* **187** 137–43

[36] Sodano H A, Lloyd J M and Inman D J 2006 An experimental comparison between several active composite actuators for power generation *Smart Mater. Struct.* **15** 1211

[37] Shahab S and Erturk A 2016 Electrohydroelastic Euler–Bernoulli–Morison model for underwater resonant actuation of macro-fiber composite piezoelectric cantilevers *Smart Mater. Struct.* **25** 105007

[38] Aloui R, Larbi W and Chouchane M 2019 Finite element reduced order model of a piezoelectric energy harvester *Proc. of the 9th ECCOMAS Conf. on Smart Structures and Materials, SMART* pp 1327–36

[39] Hamby D M 1994 A review of techniques for parameter sensitivity analysis of environmental models *Environ. Monit. Assess.* **32** 135–54

[40] Morris M D 1991 Factorial sampling plans for preliminary computational experiments *Technometrics* **33** 161–74

[41] Morris M D and Mitchell T J 1995 Exploratory designs for computational experiments *J. Stat. Plan. Inference* **43** 381–402

[42] Garcia Sanchez D, Lacarrière B, Musy M and Bourges B 2014 Application of sensitivity analysis in building energy simulations: Combining first- and second-order elementary effects methods *Energy Build.* **68** 741–50

[43] Campolongo F, Saltelli A and Cariboni J 2011 From screening to quantitative sensitivity analysis. A unified approach *Comput. Phys. Commun.* **182** 978–88

[44] Sobol' I 2001 Global sensitivity indices for nonlinear mathematical models and their Monte Carlo estimates *Math. Comput. Simul.* **55** 271–80

[45] Cunha A 2017 *Modeling and Quantification of Physical Systems Uncertainties in a Probabilistic Framework* (Cham: Springer) pp 127–56

[46] Efron B and Stein C 1981 The Jackknife estimate of variance *Ann. Statistics* **9** 586–96

[47] Metropolis N and Ulam S 1949 The monte carlo method *J. Am. Stat. Assoc.* **44** 335–41 pMID: 18139350

[48] Rubinstein R Y and Kroese D P 2017 Simulation and the Monte Carlo Method 3rd edn *Wiley Series in Probability and Statistics* (Hoboken, New Jersey: Wiley)

[49] Soize C 2017 *Uncertainty Quantification: an Accelerated Course With Advanced Applications in Computational Engineering* (New York, NY: Springer Science + Business Media) (https://doi.org/10.1007/978-3-319-54339-0)

[50] Smart material manufactures and develops advanced piezoceramic composites, https://www.smart-material.com/EH-MFC-generators.html accessed: 2019-05-20

[51] Williams R B 2004 Nonlinear mechanical and actuation characterization of piezoceramic fiber composites *PhD thesis* Virginia Polytechnic Institute and State University